Theoretical investigation of 120 Gb/s all-optical AND and OR logic gates using reflective semiconductor optical amplifiers

Amer Kotb[a,b,*] **Kyriakos E. Zoiros**[c] **Wei Li**[a,*] **and Chunlei Guo**[d,*]

[a]Chinese Academy of Sciences, Changchun Institute of Optics, Fine Mechanics, and Physics, GPL, State Key Laboratory of Applied Optics, Changchun, China

[b]University of Fayoum, Department of Physics, Faculty of Science, Fayoum, Egypt

[c]Democritus University of Thrace, School of Engineering, Department of Electrical and Computer Engineering, Lightwave Communications Research Group, Xanthi, Greece

[d]University of Rochester, Institute of Optics, Rochester, New York, United States

Abstract. The performance of all-optical (AO) logic AND and OR gates, which are realized for the first time using reflective semiconductor optical amplifiers (RSOAs) as nonlinear elements, is theoretically investigated at 120 Gb/s. The switching modules that incorporate the RSOAs and exploit their potential for AO signal processing are the Mach–Zehnder interferometer and the delayed interferometer for the AND and OR operations, respectively. A performance comparison between an RSOA and a conventional semiconductor optical amplifier (SOA) is made by examining and assessing the quality factor against the operational critical parameters, including the effect of the amplified spontaneous emission. The obtained results confirm that these Boolean functions based on RSOAs can be executed at the target data rate with better performance than if conventional SOAs were used instead. [DOI: 10.1117/1.OE.60.6.066107]

Keywords: AND logic gate; OR logic gate; reflective semiconductor optical amplifier; Mach–Zehnder interferometer; delayed interferometer.

Paper 20210277 received Mar. 15, 2021; accepted for publication May 24, 2021; published online Jun. 17, 2021.

1 Introduction

All-optical (AO) AND and OR logic gates are fundamental for the accomplishment of diverse signal processing tasks exclusively in the optical domain. The implementation of these gates in this way has been widely investigated by exploiting nonlinear effects[1–4] in semiconductor optical amplifiers (SOAs).[5–31] However, the switching rates are limited due to inherent difficulties in tailoring the SOA response. A promising alternative over standard SOAs is reflective SOAs (RSOAs), which have an antireflective coating with reflectivity well below 1×10^{-5}, i.e., practically negligible, in their front facet that strongly suppresses gain ripples[32] and a high reflectivity coating in the rear facet, as schematically shown in Fig. 1. In this device, the input signal is amplified twice through the gain medium before being reflected back to the input port. The same facet is used both for signal input injection and output extraction. The bidirectional signal propagation reduces cost and complexity as enabled by the single fiber connection and simple packaging. Moreover, RSOAs provide higher gain at lower injection currents and exhibit lower noise figure and less temperature and polarization dependency than conventional SOAs.[33] Thus, RSOAs can constitute an attractive option for executing AO Boolean operations.

The RSOA round-trip structure offers important benefits that can be leveraged by AO logic gates to obtain better performance with relaxed operating conditions compared with conventional SOAs. These benefits result exactly from the signals' double pass through the active medium, which creates favorable conditions for signal amplification and switching. More specifically, they include (a) the high optical gain at low bias currents and the easy saturation

*Address all correspondence to Amer Kotb, amer@ciomp.ac.cn; Wei Li, weili1@ciomp.ac.cn; Chunlei Guo, guo@optics.rochester.edu

0091-3286/2021/$28.00

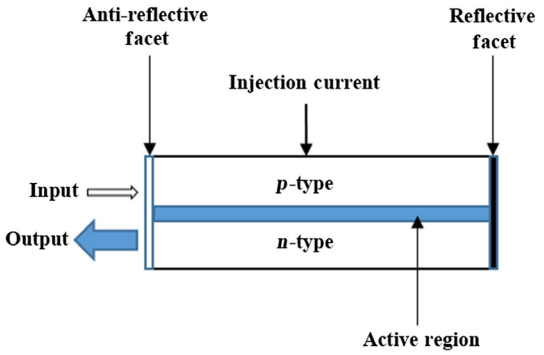

Fig. 1 Schematic of RSOA device.

at low optical powers. These properties translate into more efficient switching and practical implementation using less power-consuming current sources with less complex-associated driving electronics as well as less power hungry-and-generating erbium-doped fiber amplifiers. (b) The capability of handling input signals of a low initial power level and inherently boost the latter, so when exiting they can readily be exploited for cascadability or scalability purposes[34] without the need for extra amplification. (c) The available longer interaction length, which allows the nonlinear phase shift to be induced and accrued more effectively and hence the cross-phase modulation (XPM) effect exploited for switching to manifest more efficiently and with lower switching energy.[35,36] (d) The acceleration of the effective gain recovery time without special schemes or additional devices and thus with affordable realization and cost,[36] which allows for handling and switching ultrafast signals with enhanced performance.

Although RSOAs have been exploited for direct modulation, in the linear operating regime,[37–39] and for AO signal processing functionalities in the nonlinear operating regime,[40–43] their use for AO logic so far had been limited to the realm of implementation concept,[44,45] and only recently has their performance been thoroughly studied for this purpose.[46–48] However, these works have not studied the execution of AO AND and OR logic gates using RSOAs as nonlinear elements. Also, the approach usually followed to simulate the operation of RSOAs is computationally cumbersome as it involves solving a set of coupled partial nonlinear differential equations with boundary conditions.[49,50]

Given the current state of the art, this work aims at exploring the RSOAs potential for executing AND and OR Boolean functions by leveraging RSOAs inherent capabilities for AO switching. For this purpose, the Mach–Zehnder interferometer (MZI), which is a well-established switching module,[8,10] is used to construct the AND gate, and the delayed interferometer (DI)[5,11] is used to construct the OR gate. The approach that we adopt to model the RSOA operation and numerically study the performance of these gates at 120 Gb/s relies on a reduced model for the RSOA nonlinear behavior,[51–53] which has been formulated according to a rigorous theoretical framework.[54] To the best of our knowledge, this is the first time that the specific model is applied in the context of RSOA-based AO AND and OR logic gates. The employed model allows for calculating the RSOA response to an optical excitation from the solution of the first-order coupled differential equations in the time domain and hence greatly reduces the computational complexity without compromising the quality of the obtained results. In this paper, we aim to extend and generalize our previous research[46–48] based on using RSOAs to implement AO logic gates at 120 Gb/s. The impact of critical operating parameters, which include the RSOAs rear facet reflectivity, internal loss coefficient, length, thickness, traditional linewidth enhancement factor (α-factor), carrier lifetime, saturation power, and injection current, as well as the data signals' pulse width, pulse energy, and DI delay, on the quality factor (QF) is examined and assessed for both RSOA and conventional SOA cases while taking into account the impact of amplified spontaneous emission (ASE). The outcome of this study confirms that the AO logic AND and OR gates using RSOAs can operate at 120 Gb/s with a higher QF than if conventional SOAs were used instead. The conducted work provides a motive for employing RSOAs beyond typical areas and spurring further research on AO signal processing tasks, which have traditionally been executed using the technology of conventional SOAs. By demonstrating the feasibility of embedding RSOAs in interferometric configurations, it also contributes towards

forming a platform for designing and constructing more complex circuits and subsystems of enhanced logic functionality using the RSOA-assisted MZI as a core logic module.

2 AND and OR Gates Implementation

2.1 *Operation Principle*

To realize the Boolean AND operation, an optical data stream A at wavelength λ_1 and its delayed replica are injected via wavelength selective couplers (WSCs) into ports 1 and 3, respectively, of an RSOA-MZI, while an optical data stream B at wavelength λ_2 is injected via a 3-dB optical amplifier (OC) into port 2, as shown in Fig. 2. The WSCs combine or split signals with different wavelengths, while the 3-dB OCs combine or split signals with the same wavelength. The value of the time delay of the delayed signal A is 0.8 ps. The data A and its lagging version incur through XPM a phase change on data B. When $A = 0$, there is no such phase change, so the RSOA-MZI logical output is 0 both for $B = 1$ and $B = 0$. However, when $A = 1$ and $B = 1$, the induced phase change allows the split copies of signal B to constructively interfere at the output, producing the binary result 1 at port 2. Thus, this process produces a 1 at λ_2 only when both data A and B are 1, which is the function of the AND gate.

In the circuit of Fig. 2, there is no phase bias between RSOA1 and RSOA2 since the goal is to induce the required differential phase difference between the MZI arms by properly selecting and combining the involved critical operating parameters through numerical simulation and analysis. In practice, this task can be facilitated by employing after each RSOA active phase shifters, which provide an extra phase difference between the upper and lower MZI arms[55] for achieving switching. From a technological perspective, these shifters are thermo-optic elements that feature low tuning voltage and power dissipation[56] and can be embedded with SOA-based devices in the same planar lightwave circuit platform.[57]

To realize the Boolean OR operation, the optical data streams A and B and a continuous wave (CW) probe signal are injected into the RSOA-DI, as shown in Fig. 3. These signals are spectrally located at different wavelengths that fall within the C-band fiber transmission window, e.g., 1555, 1553, and 1557 nm, respectively, so they can be properly discriminated from each other. Data A and B induce via XPM a phase change on the CW signal inside the RSOA. The, the CW signal that comes out of the RSOA is injected into a DI that has a relative delay ($\Delta\tau$) in one of its arms and a phase bias ($\Delta\Phi$) in the other arm. The value of $\Delta\tau$ used in the simulation is 0.2 ps. The DI creates a phase difference between the direct and the temporally offset versions of the CW signal that emerges from the RSOA and on which the dynamic perturbations by A and B have been mapped. This action opens a phase window[58] with a duration that is solely determined by the DI relative delay, which is much smaller than the target repetition period. This allows the processed pulses to preserve the quality of their original profile despite the RSOA being heavily saturated in the tight driving scenario when both data signals must be sufficiently strong to efficiently excite the exploited RSOA nonlinearity. Thus, if $A = 0$ and $B = 0$, there is no phase

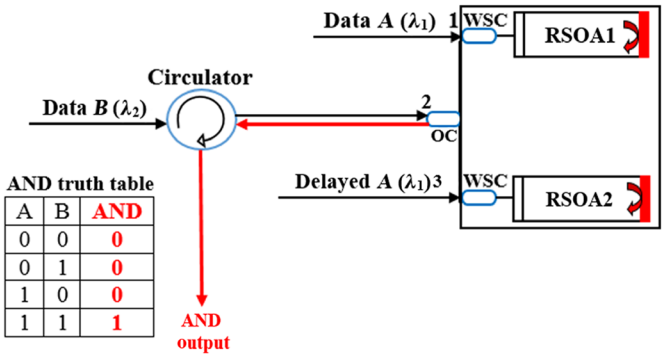

A	B	AND
0	0	0
0	1	0
1	0	0
1	1	1

Fig. 2 Schematic diagram and truth table of Boolean AND operation using RSOA-MZI. OC, 3-dB optical coupler; WSC, wavelength-selective coupler.

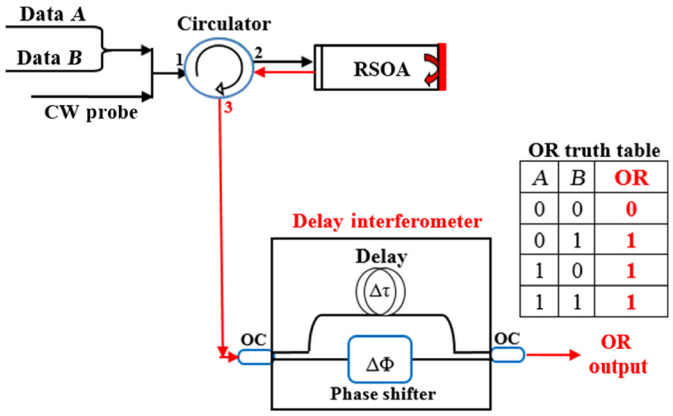

Fig. 3 Schematic diagram and truth table of Boolean OR operation using RSOA-DI. $\Delta\tau$, relative delay; $\Delta\Phi$, phase bias.

change on the CW signal and accordingly no phase window opening, which results in no output, i.e., 0, from the DI. However, in the presence of either A or B, or both, i.e., $A = 1$ and $B = 0$ or vice versa, and $A = B = 1$, respectively, phase changes are incurred on the CW signal that exits the RSOA. Although these phase changes are stronger in the latter than in the former binary combination, the induced phase excursions induced in both cases can be arranged through the proper choice of the DI delay to lie within the formed phase window and around the same average level. This is done by adjusting the DI phase bias to π, so the straightforward and lagging counterparts of the CW signal interfere destructively at the DI cross output port. In this manner, and despite the different degree of RSOA saturation, an output of almost equal magnitude is obtained, which coincides with the logical outcome of the Boolean OR function.

2.2 *Simulation*

Based on the analytical models developed in Refs. 52 and 53, the time-dependent gain perturbed inside the RSOAs is derived by numerically solving the following first-order coupled differential equation:[46–48]

$$\frac{\mathrm{d}h_{CD}(t)}{\mathrm{d}t} = \frac{(\ln G_0/2) - h_{CD}(t)}{\tau_c} - \frac{h_{\mathrm{CD}}(t)}{h_{\mathrm{CD}}(t) - \alpha_{\mathrm{loss}}L}(\exp[h_{\mathrm{CD}}(t) + h_{\mathrm{CH}}(t) + h_{\mathrm{SHB}}(t) - \alpha_{\mathrm{loss}}L] - 1)$$
$$(1 + R\,\exp[h_{\mathrm{CD}}(t) + h_{\mathrm{CH}}(t) + h_{\mathrm{SHB}}(t) - \alpha_{\mathrm{loss}}L])\frac{P_{\mathrm{in}}(t)}{E_{\mathrm{sat}}}, \quad (1)$$

$$\frac{\mathrm{d}h_{\mathrm{CH}}(t)}{\mathrm{d}t} = -\frac{h_{\mathrm{CH}}(t)}{\tau_{\mathrm{CH}}} - \frac{\varepsilon_{\mathrm{CH}}}{\tau_{\mathrm{CH}}}(\exp[h_{\mathrm{CD}}(t) + h_{\mathrm{CH}}(t) + h_{\mathrm{SHB}}(t) - \alpha_{\mathrm{loss}}L] - 1)$$
$$(1 + R\exp[h_{\mathrm{CD}}(t) + h_{\mathrm{CH}}(t) + h_{\mathrm{SHB}}(t) - \alpha_{\mathrm{loss}}L])P_{\mathrm{in}}(t), \quad (2)$$

$$\frac{\mathrm{d}h_{\mathrm{SHB}}(t)}{\mathrm{d}t} = -\frac{h_{\mathrm{SHB}}(t)}{\tau_{\mathrm{SHB}}} - \frac{\varepsilon_{\mathrm{SHB}}}{\tau_{\mathrm{SHB}}}(\exp[h_{\mathrm{CD}}(t) + h_{\mathrm{CH}}(t) + h_{\mathrm{SHB}}(t) - \alpha_{\mathrm{loss}}L] - 1)$$
$$(1 + R\exp[h_{\mathrm{CD}}(t) + h_{\mathrm{CH}}(t) + h_{\mathrm{SHB}}(t) - \alpha_{\mathrm{loss}}L])P_{\mathrm{in}}(t) - \frac{\mathrm{d}h_{\mathrm{CD}}(t)}{\mathrm{d}t} - \frac{\mathrm{d}h_{\mathrm{CH}}(t)}{\mathrm{d}t}, \quad (3)$$

where $h_{\mathrm{CD}}(t)$, $h_{\mathrm{CH}}(t)$, and $h_{\mathrm{SHB}}(t)$ stand for the RSOAs gains integrated over their active region length and induced during the dynamic processes of carrier depletion (CD), carrier heating (CH), and spectral hole burning (SHB), respectively. G_0 is the unsaturated power gain, R is the rear facet reflectivity, α_{loss} is the internal optical loss coefficient, and L is the length of the RSOAs active region. $P_{\mathrm{in}}(t)$ is the total power of the signals inserted in the RSOAs according to each case of the considered Boolean operation. $E_{\mathrm{sat}} = P_{\mathrm{sat}}\tau_c$ is the RSOAs saturation energy, where P_{sat} is the saturation power and τ_c is the carrier lifetime. E_{sat} is linked to the confinement

factor (Γ) through $E_{sat} = Ah\upsilon/a\Gamma$,[22] where A is the cross-section area of the active region, i.e., $A \cong wd$ (w and d are the width and thickness of the active layer, respectively), $h\upsilon$ is the signal photon energy, and a is the differential gain. τ_{CH} and τ_{SHB} are the temperature relaxation rate and the carrier–carrier scattering rate, respectively. ε_{CH} and ε_{SHB} are the nonlinear gain suppression factors due to CH and SHB, respectively.

The total nonlinear gain $G(t)$ of each RSOA is given by[46–48]

$$G(t) = R\ \exp[2(h_{CD}(t) + h_{CH}(t) + h_{SHB}(t) - \alpha_{loss}L)], \tag{4}$$

where the multiplicative factor "2" at the front of the exponential argument takes into account the double pass of the signal inside the RSOAs active region.

The phase change incurred on the signal propagating through the RSOAs is given by[46–48]

$$\Phi(t) = -(\alpha h_{CD}(t) + \alpha_{CH}h_{CH}(t) + \alpha_{SHB}h_{SHB}(t)), \tag{5}$$

where α is the traditional linewidth enhancement factor (α-factor) and α_{CH} and α_{SHB} are the linewidth enhancement factors due to CH and SHB, respectively. The value of α_{SHB} is zero because SHB produces a symmetrical spectral hole centered at the signal wavelength.[59]

For both AND and OR operations, the input powers of data A and B are assumed to be Gaussian-shaped with full-width at half-maximum (FWHM) pulse width (τ_{FWHM}), input pulse energy (E_0), bit period (T_{per}), and length of the pseudorandom binary sequence (PRBS) $N = 2^7 - 1$,[46–48]

$$P_{A,B}(t) \equiv P_{in}(t) = \sum_{n=1}^{N} a_{n(A,B)}\ \frac{2\sqrt{\ln[2]}E_0}{\sqrt{\pi}\tau_{FWHM}}\ \exp\left[-\frac{4\ \ln[2](t - nT_{per})^2}{\tau_{FWHM}^2}\right], \tag{6}$$

where $\alpha_{n(A,B)}$ denotes the n'th pulse inside the PRBS, which can take the logical value 1 or 0. For the AND operation, the input powers inside the RSOAs, which are symmetrically placed in each MZI arm, are expressed by

$$P_{in,RSOA\,1}(t) = P_A(t) + 0.5P_B(t), \tag{7}$$

$$P_{in,RSOA\,2}(t) = P_{delayed\,A}(t) + 0.5P_B(t), \tag{8}$$

where the coefficient 0.5 accounts for the coupling into the switching configuration of data signal B via the appropriate passive component. For the OR operation, the optical power going inside the RSOA-DI is given by

$$P_{in,RSOA\text{-}DI}(t) = P_A(t) + P_B(t) + P_{CW}. \tag{9}$$

The output power of the AND gate is described by[19,22]

$$\begin{aligned} P_{AND}(t) = {} & 0.25P_B(t)(G_{RSOA1}(t) + G_{RSOA2}(t) \\ & - 2\sqrt{G_{RSOA1}(t)G_{RSOA2}(t)}\cos[\Phi_{RSOA1}(t) - \Phi_{RSOA2}(t)]), \end{aligned} \tag{10}$$

where $G_{ROSA1,2}(t)$ and $\Phi_{RSOA1,2}(t)$ are the time-dependent total gains and phase shifts induced inside RSOA1 and RSOA2, respectively. The output power of the OR gate is described by[58]

$$\begin{aligned} P_{OR}(t) = 0.25\Big(& P_{out,RSOA}(t) + P_{out,RSOA}(t - \Delta\tau) \\ & - 2\sqrt{P_{out,RSOA}(t)P_{out,RSOA}(t - \Delta\tau)}\cos[\Phi(t) - \Phi(t - \Delta\tau)]\Big), \end{aligned} \tag{11}$$

where $P_{out,RSOA}(t) = G(t)\ P_{CW}$ and $\Phi(t) - \Phi(t - \Delta\tau)$ is the differential phase introduced by the DI. The RSOAs ASE acts as noise, the effect of which can be accounted for by adding numerically to the output power of the AND or OR the ASE power (P_{ASE}), which is calculated from the following equation:[17,60]

$$P_{\mathrm{ASE}} = N_{\mathrm{sp}}(G_0 - 1)2\pi\hbar\upsilon B_0, \tag{12}$$

where N_{sp} is the spontaneous emission factor, $\hbar$ is the normalized Planck's constant, and B_0 is the optical bandwidth at an optical frequency (υ) in the vicinity of 1550 nm. To improve the performance of both considered gates, the critical operating parameters that have been identified at the end of Sec. 1 should be optimized by means of numerical simulations. The default values of these critical parameters used in these simulations are given in Table 1.

3 Results

For a 120-Gb/s input optical signal, Fig. 4 depicts the gain dynamics of both the RSOA and the conventional SOA. Due to the signal double pass, the RSOA is saturated more heavily than the conventional SOA. Moreover, due to the enhanced effective gain recovery time, the RSOA responds in a more uniform manner to rapid changes of the incoming data, in comparison with the conventional SOA, which has a slower response that suffers from the pattern effect, i.e., peak amplitude fluctuations. This indicates that the RSOA could be favorably exploited for high-speed AO logic purposes.

The performance of the AO AND and OR logic gates is investigated and evaluated by means of the QF metric, which is defined as $\mathrm{QF} = (P_1 - P_0)/(\sigma_1 + \sigma_0)$,[46–48] where $P_{1,0}$ are the mean peak powers of the logical 1s and 0s expected at the outputs of the RSOA-MZI or the RSOA-DI and $\sigma_{1,0}$ are the corresponding standard deviations. For acceptable performance, the QF must be over 6 to keep the relevant bit error rate less than 10^{-9}.[22] We also calculated the extinction ratio (ER) value to further check and confirm the correct operation and high performance of the logic schemes. The ER is defined as the ratio of the minimum and maximum power between the logical 1s and 0s, i.e., $\mathrm{ER(dB)} = 10\log[P^1{}_{\mathrm{min}}/P^0{}_{\mathrm{max}}]$, and it should be over 10 dB.[34] The conducted simulations reveal that, if designed as suggested according to the interpretation of the variation of the critical operating parameters against the QF, which is presented in the following, the achieved QF and ER based on RSOAs are 28 and 13.4 dB for the AND operation, respectively, and 17 and 11.5 dB for the OR operation, respectively. The simulated temporal profiles and eye diagrams for the AND and OR operations are depicted in Figs. 5 and 6, respectively. These figures confirm that both Boolean functions are executed at 120 Gb/s with logical correctness and good quality.

The variations in the output logic 1 level observed in both AND and OR logic operations are physically attributed to (a) the RSOAs finite carrier lifetime, which is quite longer than the signal repetition period, so the RSOAs gain, after being perturbed by the input excitation, cannot timely recover to the same initial level for the next data pulse. As a result, the gain experienced by each incoming pulse depends not solely on its content but also on the RSOAs response to the preceding pulses.[64] This situation affects analogously the induced phase shift, and thus the switched output becomes pattern-dependent, which is visualized as unequal pulse peak amplitudes. (b) The noise contribution due to RSOAs ASE, which shifts and essentially disturbs the output power level that already has been impaired by the effect in (a), to an extent that it aggravates the peak amplitude fluctuations of the logical outcomes. Because the logical outcome of the OR operation contains, by definition, more logical 1s than the AND operation for the same number of input binary combinations, the OR operation is more prone to pattern effects than the AND, and for this reason the peak amplitude fluctuations are more discernible for the former than for the latter Boolean function. This discrepancy is also mapped on the corresponding eye diagrams, which for the AND has a single border of imperceptible envelopes, while for the OR it comprises two envelopes with a peak amplitude difference that is a direct product of the stronger impact of the pattern effects. Nevertheless, the performance of both AND and OR operations is not irreversibly harmed, as quantified by the amplitude modulation defined by the ratio of the maximum to the minimum switched pulse peak amplitudes, which remains below 1 dB and hence is acceptable. [65]

Figures 7–16 depict a set of simulations results for the influence of the input signals and RSOAs physical and structural characteristics on the QF. To help understand the trends of the QF, curves of the corresponding induced phase difference have been plotted along with the QF

Table 1 Critical parameters and their default values for simulation of AND and OR operations.

Symbol	Definition	Value	Unit	Ref(s).
E_0	Pulse energy	0.01	pJ	19
τ_{FWHM}	Pulse width	1	ps	47–49
T	Bit period	8.33	ps	47–49
n	PRBS length	127	—	11, 21
R	Rear facet reflectivity	1	—	52
α_{loss}	Internal loss coefficient	10	mm^{-1}	47
λ_A	Wavelength of data A (AND operation)	1580.4	nm	29
$\lambda_{delayed\,A}$	Wavelength of delayed A (AND operation)	1580.4	nm	29
λ_B	Wavelength of data B (AND operation)	1539.8	nm	29
P_A	Power of data A (AND operation)	0.4	mW	29
$P_{delayed\,A}$	Power of delayed A (AND operation)	0.4	mW	29
P_B	Power of data B (AND operation)	0.001	mW	29
$\Delta\tau$	Time delay (AND operation)	0.5	ps	—
λ_A	Wavelength of data A (OR operation)	1581	nm	5, 11, 12, 15
λ_B	Wavelength of data B (OR operation)	1581	nm	5, 11, 12, 15
λ_{CW}	Wavelength of CW (OR operation)	1540	nm	5, 11, 12, 15
P_A	Power of data A (OR operation)	1	mW	5, 11, 12, 15
P_B	Power of data B (OR operation)	1	mW	5, 11, 12, 15
P_{CW}	Power of CW (OR operation)	2	mW	5, 11, 12, 15
$\Delta\tau_{DI}$	DI delay (OR operation)	0.2	ps	—
$\Delta\Phi$	DI phase bias (OR operation)	π	rad	5, 11, 12, 15
λ_{WSC}	WSC wavelength	1550	nm	61
P_{WSC}	WSC coupled power	−10	dBm	61
I	Injection current	100	mA	47, 62
P_{sat}	Saturation power	15	mW	47
τ_c	Carrier lifetime	100	ps	47, 62
α	Traditional linewidth enhancement factor	6	—	62
α_{CH}	Linewidth enhancement factor due to CH	1	—	19, 22
α_{SHB}	Linewidth enhancement factor due to SHB	0	—	19, 22
ε_{CH}	Nonlinear gain suppression factor due to CH	0.02	W^{-1}	19, 22
ε_{SHB}	Nonlinear gain suppression factor due to SHB	0.02	W^{-1}	19, 22
τ_{CH}	Temperature relaxation rate	0.3	ps	47
τ_{SHB}	Carrier–carrier scattering rate	0.1	ps	47
Γ	Confinement factor	0.15	—	10, 62
a	Differential gain	8.6×10^{-15}	cm^{-2}	63
L	Length of RSOA active layer	0.4	mm	47
d	Thickness of RSOA active layer	0.3	μm	24, 47
G_0	Unsaturated power gain	15	dB	47
N_{SP}	Spontaneous emission factor	2	—	17, 62
B_0	Optical bandwidth	2	nm	17, 62

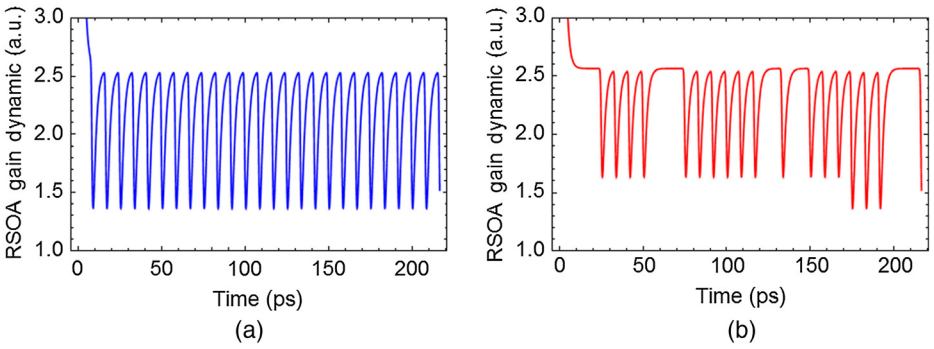

Fig. 4 Gain dynamic for RSOA and SOA at 120 Gb/s.

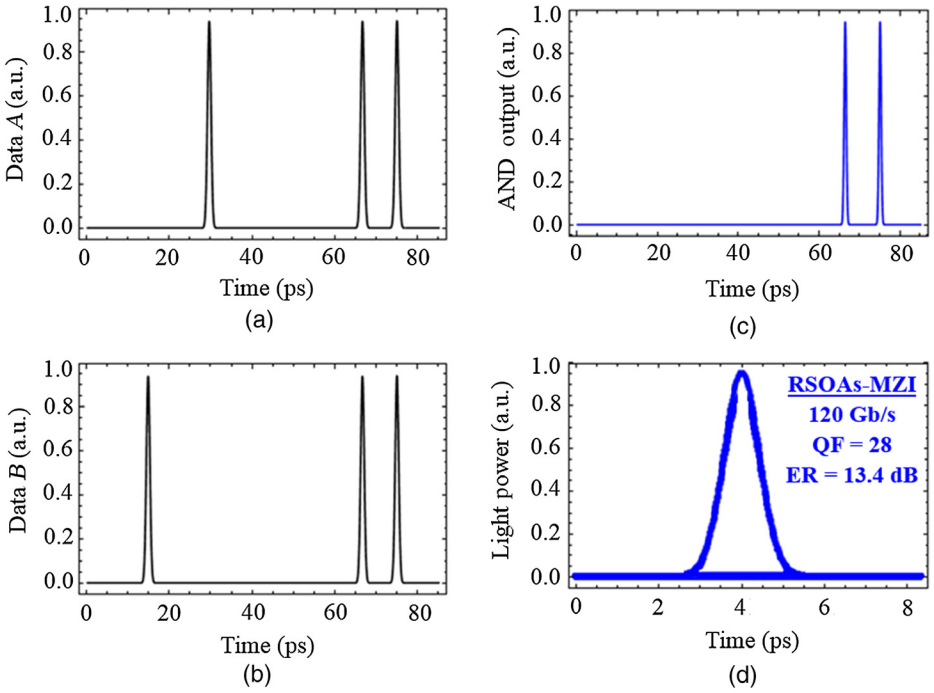

Fig. 5 Simulation results for AND operation using RSOA-MZI at 120 Gb/s. (a) Input data *A*, (b) input data *B*, (c) output AND gate, and (d) AND eye diagram.

ones. In all cases, the variation of the QF is the opposite of that of the induced phase difference, which can be qualitatively explained according to the details given in Ref. 66.

The QF versus the RSOAs rear facet reflectivity for different values of the data *A* input powers is shown in Fig. 7, which reveals that a minimum value of 25% and 60% is required for this parameter with regard to the AND and OR operations, respectively. This minimum is dictated by the fact that the dynamically perturbed signal inside the RSOA should be efficiently reflected by the RSOA rear facet, so the gain it perceives is brought to a level sufficient for switching.[66] Since the OR operation is logically and physically more demanding than the AND operation, this minimum is higher for the former than for the latter operation, but in both cases, it is practically achievable.

Figure 8 shows the QF as a function of the RSOAs internal loss coefficient for different injection currents. From Fig. 8(a), it can be seen that although the QF is decreased as internal losses become higher, yet for both Boolean operations this effect is not detrimental and can be well compensated for by providing more carriers, at the cost of increased power consumption. A different behavior is observed in Fig. 8(b), in which the internal loss coefficient decreases as the phase difference value increases.

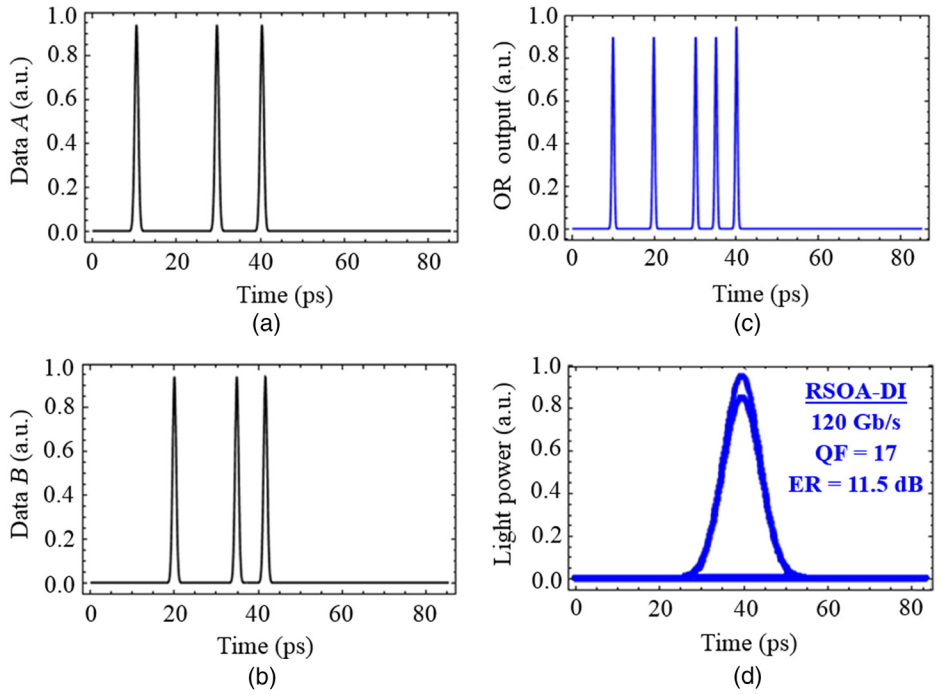

Fig. 6 Simulation results for OR operation using RSOA-DI at 120 Gb/s. (a) Input data *A*, (b) input data *B*, (c) output OR gate, and (d) OR eye diagram.

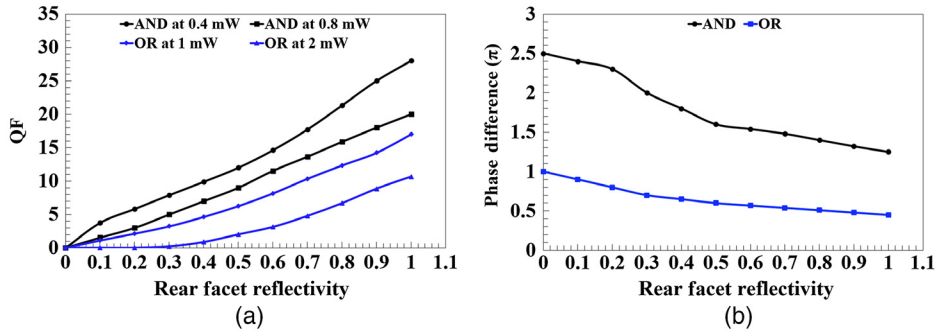

Fig. 7 (a) QF versus RSOAs rear facet reflectivity for RSOA-based AND and OR operations and (b) phase difference versus RSOAs rear facet reflectivity for AND and OR operations.

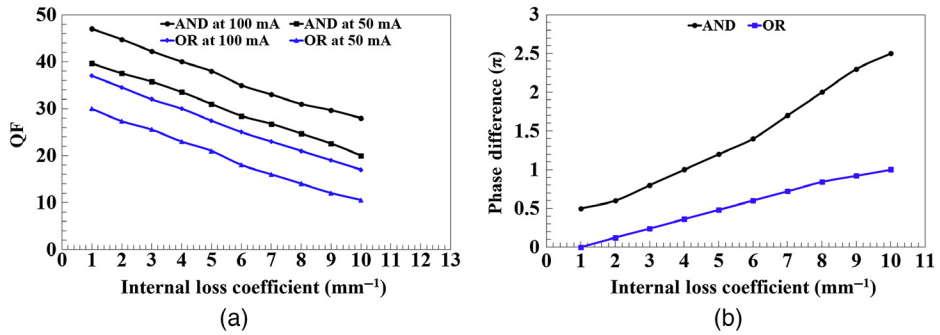

Fig. 8 (a) QF versus RSOAs internal loss coefficient at two different values of injection current and (b) phase difference versus internal loss coefficient for AND and OR operations at 100 mA.

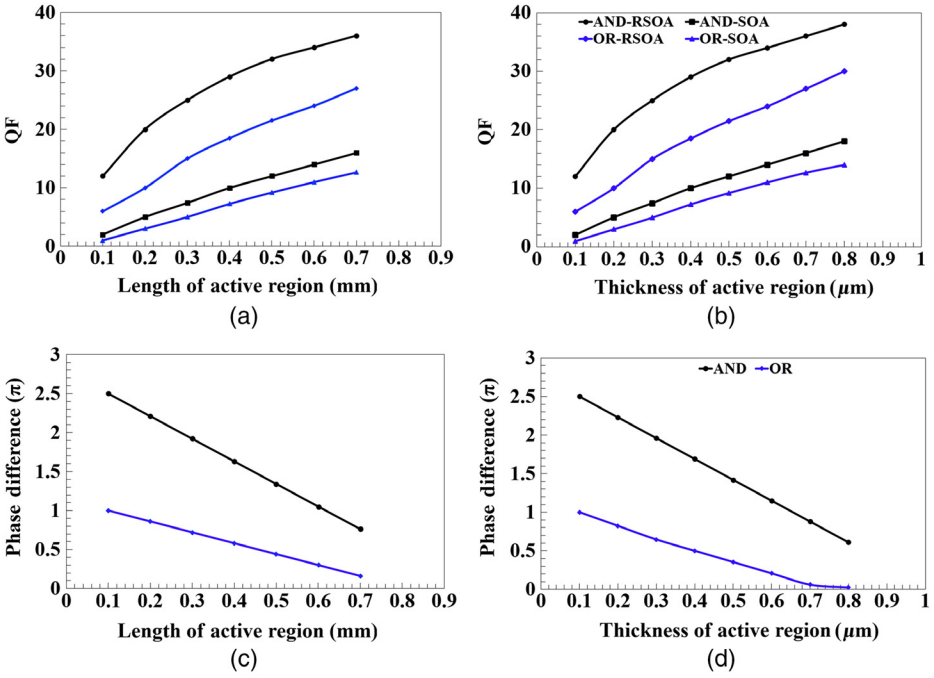

Fig. 9 QF versus (a) length and (b) thickness for RSOA and conventional SOA-based AND and OR operations. Phase difference versus (c) length and (d) thickness for RSOA-based AND and OR operations.

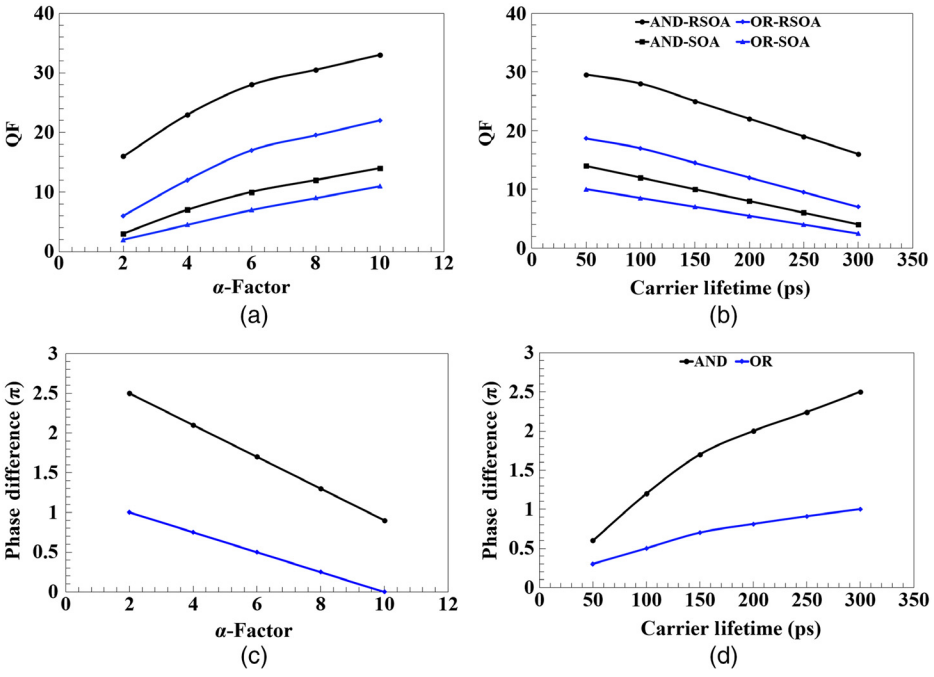

Fig. 10 QF versus (a) α-factor and (b) carrier lifetime for RSOA and conventional SOA-based AND and OR operations. Phase difference versus (c) α-factor and (d) carrier lifetime for RSOA-based AND and OR operations.

The dependence of the QF on the length and thickness of the RSOA in comparison with the conventional SOA is shown in Figs. 9(a) and 9(b), respectively. Generally, the QF becomes higher for longer and thicker optical amplifiers. The double-pass RSOA device allows for enough space to induce more strongly the nonlinear phase shift required for switching.[35]

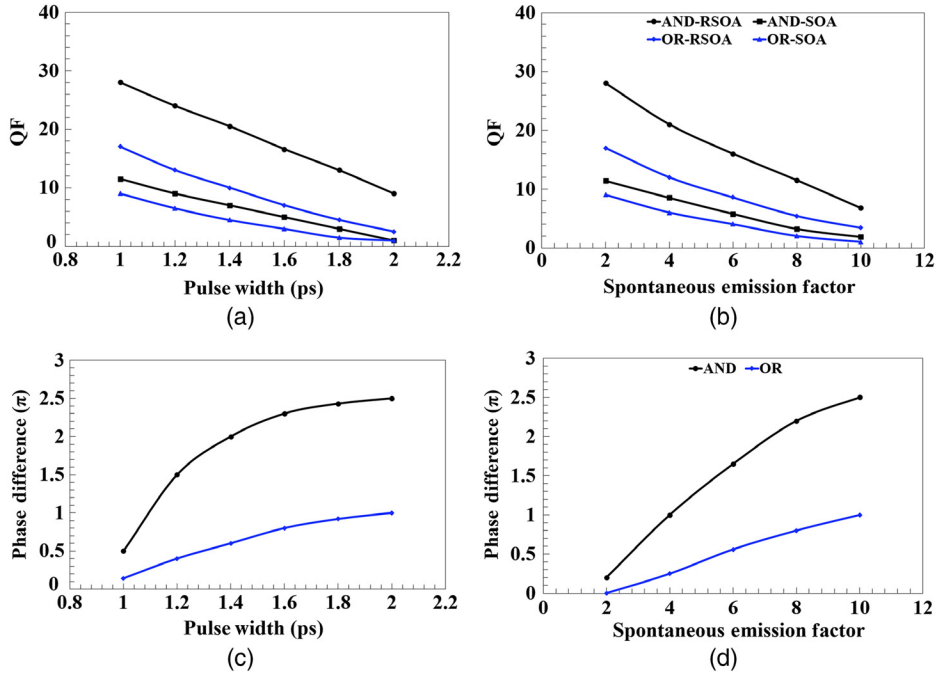

Fig. 11 QF versus (a) pulse width and (b) spontaneous emission factor for RSOA and conventional SOA-based AND and OR operations. Phase difference versus (c) pulse width and (d) spontaneous emission factor for RSOA-based AND and OR operations.

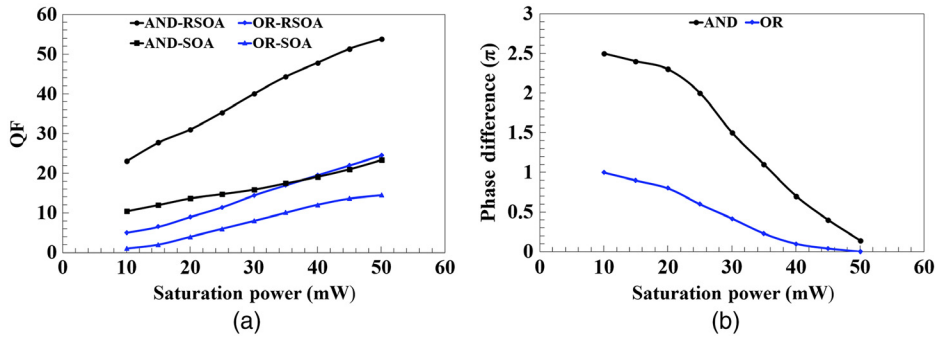

Fig. 12 (a) QF versus saturation power for RSOA and conventional SOA-based AND and OR operations. (b) Phase difference versus saturation power for RSOA-based AND and OR operations.

Thus, the QF achieved with the longest SOA is almost the same as that with the shortest RSOA for the same Boolean operation. A similar observation is made with regard to the thickness of the active region of these devices. The main conclusion derived from these results is that the performances of AO logic AND and OR gates are acceptable using RSOAs with a size that is more compact than that of their standard counterparts.

The dependence of the QF on the traditional linewidth enhancement factor (α-factor) and the carrier lifetime (τ_c) for the AND and OR operations is shown in Fig. 10, which has been derived for the RSOA and the standard SOA. As shown in Fig. 10(a), the QF is increased with the α-factor due to the effect that this parameter has on the induced phase change and accordingly on the magnitude of switching.[67] Moreover, for the RSOA-based logic schemes, the QF is acceptable for both Boolean functions for a smaller α-factor than for the standard SOA-based. Similarly, for the same α-factor, the QF is higher for the RSOA than for the SOA case. Since the α-factor depends on the operating conditions,[53,67] the latter can be relaxed, which is highly desirable from a practical standpoint. On the other hand, the carrier lifetime plays an important role in RSOA-based AO signal processing. Generally, for a long carrier lifetime against the pulse repetition period,

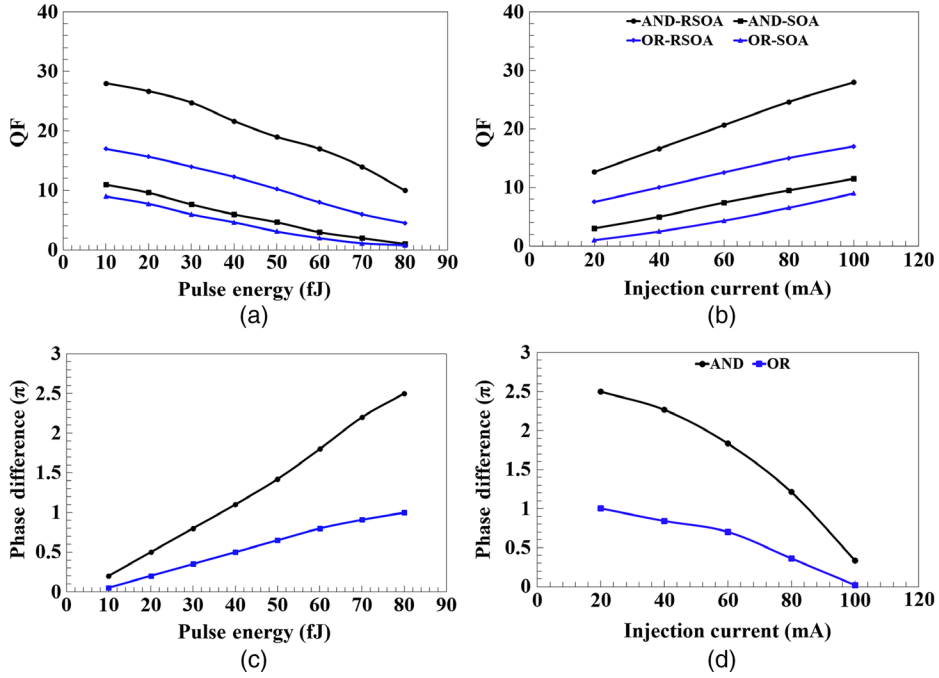

Fig. 13 QF versus (a) pulse energy and (b) injection current for RSOA and conventional SOA-based AND and OR operations. Phase difference versus (c) pulse energy and (d) injection current for RSOA-based AND and OR operations.

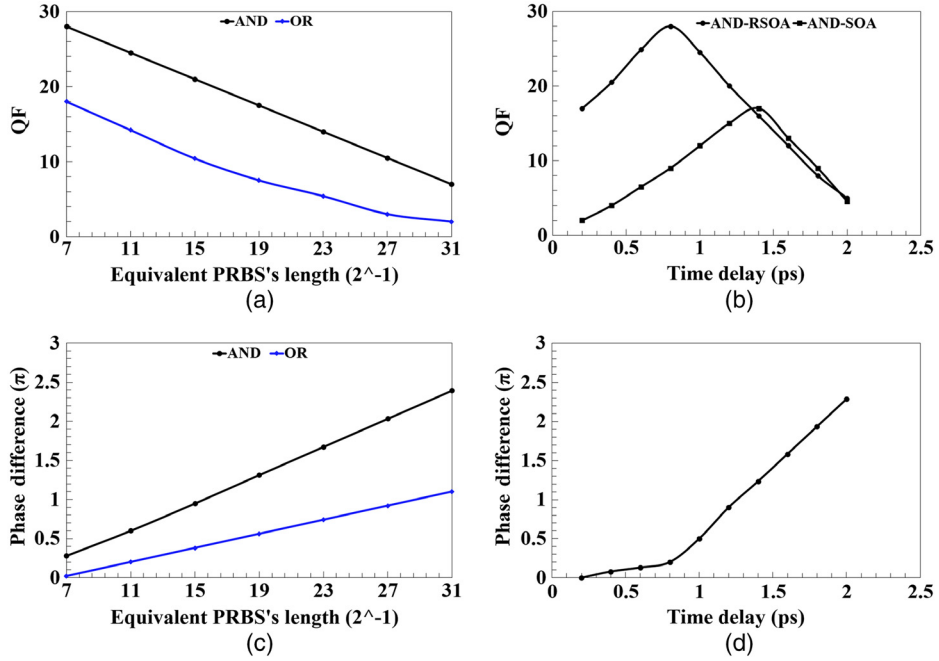

Fig. 14 QF versus (a) equivalent PRBS's length for RSOA-based AND and OR operations and (b) time delay of data signal *A* for RSOA-based and SOA-based AND operations. Phase difference versus (c) equivalent PRBS's length for RSOA-based AND and OR operations and (d) time delay of data signal *A* for RSOA-based AND operation.

the carriers' density will slowly be replenished, which is a cause of pulse distortion that limits the maximum operating data rate. Figure 10(b) shows indeed that the QF is decreased as the carrier lifetime becomes higher. Nevertheless, owing to the assistance by the external delay, either of one of the data signals in the AND operation, or the DI in the OR operation, the constraining

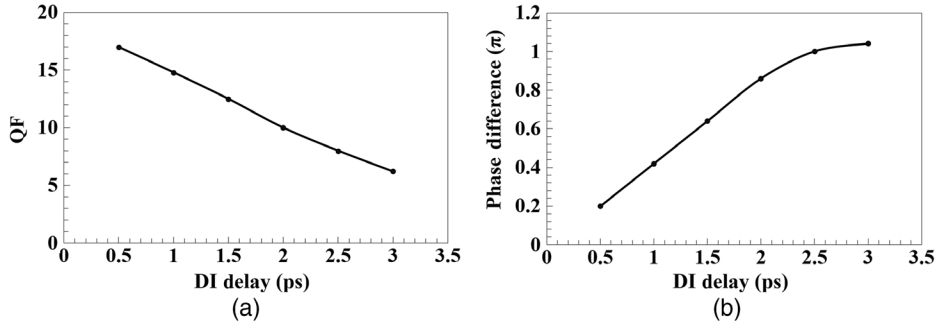

Fig. 15 (a) QF versus DI delay and (b) phase difference vs. DI delay for RSOA-based OR operation.

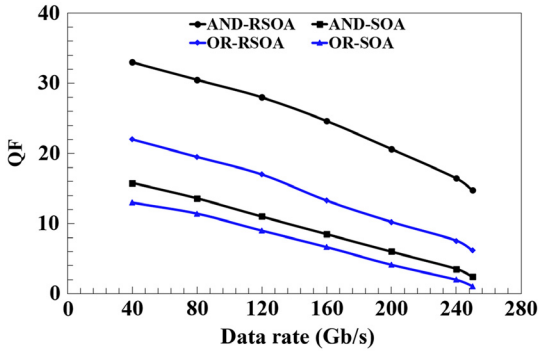

Fig. 16 QF versus data rate for AND and OR operations using RSOA and conventional SOA.

impact of the carrier lifetime can be effectively masked. Thus, for both Boolean functions, the QF remains acceptable for a carrier lifetime that is allowed to exceed by multiple times the pulse repetition interval, while this happens more conveniently for the RSOA than for the SOA.

The QF is affected by the pulse width (τ_{FWHM}) and the (R)SOAs' ASE. Figure 11(a) shows that the QF is decreased as pulses become broader. This happens because pulse becomes more energetic (for a given peak power), which causes a stronger saturation of the RSOAs that impairs the switching procedure and outcome. Still, the QF is more tolerant to the variations of the specific temporal parameter for the RSOA since for both Boolean operations it is allowed to vary by at least 40% beyond the maximum pulse width permitted for the SOA. This means that preferring RSOAs over SOAs can relax the requirements for the implementation of the optical sources that generate the data pulses. Figure 11(b) shows the QF versus the spontaneous emission factor for an optical bandwidth $B_0 = 2$ nm. The ASE affects the QF of the RSOA-based scheme less than that of the conventional SOA-based scheme. Despite the ASE, high QF values are possible by the inherently longer RSOA interaction length and high rear-facet reflectivity, owing to which the nonlinear phase shift required for switching is induced and accrued more efficiently.[36] This indicates that employing RSOAs as nonlinear elements can be advantageous when combining the considered AO gates to form more complex circuits of enhanced functionality.

The QF as a function of the saturation power for the RSOA- and conventional SOA-based AND and OR operations is shown in Fig. 12. It is seen that the QF becomes acceptable for a lower saturation power when using RSOA instead of SOA. Physically, this fact is attributed to the different way and strength that gain saturation is realized in the two types of devices, which in turn is a direct by-product of their construction and operation.[68] Consequently, AO switching can be achieved in a more power-efficient manner for the RSOA than for the SOA, which favors the use of the former over the latter.

The QF dependence on the input pulse energy and (R)SOAs injection current is shown in Figs. 13(a) and 13(b), respectively. From Fig. 13(a), it is seen that for the RSOA-based schemes the QF of both logic operations remains acceptable nearly across the whole scanned range of

input pulse energy, something that is not possible with the SOA-based ones. Additionally, better performance is achieved with the RSOA than with the SOA for the same pulse energy, which hence can be lower and affordably provided by low cost and power consuming erbium-doped fiber amplifiers. These attractive features offered using the RSOA are enabled by the feedback process that occurs inside the RSOA cavity and maximizes the perturbation of the offered gain. On the other hand, the QF is increased as more carriers are supplied via higher bias currents, as shown in Fig. 13(b). Moreover, the injection current required to obtain a given high QF for the Boolean functions is a few tens of mAs with the RSOA as opposed to over hundreds of mAs with the SOA. This fact is critical for the practical implementation of both logic gates since the switching configurations that incorporate RSOAs can be driven using less complex and power-consuming electronic circuitry.

Figure 14(a) shows the dependence of the QF on the equivalent length[69] of the PRBS carried by the input data for AND and OR operations with RSOAs. As seen, the performance of both Boolean functions is acceptable for equivalent PRBS lengths on the order of 23, which is fairly high for fully capturing the pattern effects and accurately calculating the QF of ultrafast (R)SOA-based AO switching.[64] The time delay between data A and its time-shifted version is a very critical parameter for the operation and performance of the AND gate. Figure 14(b) shows that the double-pass RSOA can better accommodate this temporal offset than its single-pass SOA counterpart. Indeed, not only is the QF higher with the RSOA but also the peak of this metric occurs at almost half the delay than with the SOA. This reduces the unavoidable latency for buffering, preparing, and launching of delayed signal A when the latter is not locally available, as is usually the case, and accordingly facilitates real-time AO signal processing.

The key parameter for the RSOA-DI that realizes the OR function is the DI delay. Figure 15(a) shows indeed that the QF is sensitive to small changes of this parameter. Furthermore, a shorter delay, which falls well within the resolution of off-the-shelf DI modules, increases the QF, so the best performance is obtained as the delay tends closer to the pulse FWHM.

On the other hand, the time that must elapse for the first pulse that enters the RSOA to be reflected back and encounter the maximum possible gain available for switching is $T_{\text{transit}} + T_{\text{transit}}/2 = 6$ ps,[52] where $T_{\text{transit}} = 4$ ps is the single-pass transit time that corresponds to the 0.4-mm-long RSOA cavity used in the simulations. In this case, the forthcoming pulse heading in the forward direction from the RSOA front facet to the RSOA center will not have reached and traveled past this point but will need 4.3 ps more since it lags behind by $T_{\text{per}} + T_{\text{transit}}/2$. The carrier density (gain) is higher at the center of the RSOA rather than at the RSOA antireflective and reflective facets, where gain saturation by the counter-propagating fields is stronger.[52,68] In this manner, the RSOA gain dynamics will be perturbed fully and in proper pulse temporal order without being affected by the RSOA round-trip delay. Thus, as long as the repetition period exceeds the one-way propagation time, AO Boolean functionalities, such as those considered in this paper, can be achieved at speeds as fast as inversely proportional to T_{transit}. This requirement sets an upper limit on the ultrafast operation capability, which for the RSOAs longitudinal dimension employed in this paper is 250 Gb/s. Then Fig. 16 shows that, despite being decreased, the QF remains acceptable up to this data rate for both AND and OR operations when these are executed using the RSOA-based scheme, while this is not possible with conventional SOAs.

Finally, the main factors for the experimental demonstration of the logic gates schemes are those that concern the practical availability of the data signals and RSOAs. According to the simulation results, the data signals must have the appropriate intensity level, pulse width, and format at an excessively high data rate. This means that they should be generated by laser systems and boosted by erbium-doped fiber amplifiers before being launched into the AO gates, which lies well within the capabilities of the relevant state-of-the-art technology.[32,70] Similarly, the RSOAs must have such physical and structural characteristics that are affordable by off-the-shelf devices and hence are technologically feasible.[71] The experimental demonstrations have so far employed RSOAs either as intensity modulators[37–39] or for nonlinear switching functionalities other than AO logic.[40–44] This means that there is margin available for exploring the RSOAs potential for the specific functionality, so the work presented in this paper advances the knowledge in the treated research field by constituting a reference point for considering and exploiting

RSOAs as key enabling modules for the efficient manipulation of digital information exclusively in the optical domain.

4 Conclusion

In conclusion, the performance of AO logic AND and OR gates implemented using RSOAs as nonlinear elements has been theoretically investigated and extensively analyzed at 120 Gb/s. The obtained results confirm that these gates can be realized with the RSOA-assisted MZI or RSOA-DI, respectively, both with logical correctness and good quality at the target data rate. Moreover, the ultrafast execution of these fundamental Boolean functions entirely in the optical domain is technologically feasible and can be achieved with better performance as well as less demanding operating conditions than if conventional SOAs were used instead.

Acknowledgments

Amer Kotb sincerely thanks the CAS President's International Fellowship Initiative (Grant No. 2019FYT0002) and the Talented Young Scientist Program supported by the China Science and Technology Exchange Center of Ministry of Science and Technology of China. The authors report no conflicts of interest.

References

1. S. Singh and R. S. Kaler, "Minimization of cross gain saturation in wavelength division multiplexing by optimizing differential gain in semiconductor optical amplifiers," *Fiber Integr. Opt.* **25**, 287–303 (2006).
2. S. Singh and R. S. Kaler, "Wide band optical wavelength converter based on four wave mixing using optimized semiconductor optical amplifier," *Fiber Integr. Opt.* **25**, 213–230 (2006).
3. S. Singh and R. S. Kaler, "Analysis and minimization of cross phase modulation in semiconductor optical amplifiers for multichannel WDM optical communication systems," *Opt. Commun.* **274**, 105–115 (2007).
4. S. Singh, X. Ye, and R. S. Kaler, "All optical wavelength conversion based on cross polarization modulation in semiconductor optical amplifier," *IEEE J. Lightwave Technol.* **31**, 1783–1792 (2013).
5. H. Dong et al., "Demonstration of all-optical logic OR gate using semiconductor optical amplifier-delayed interferometer," *Opt. Commun.* **242**, 479–485 (2004).
6. N. K. Dutta et al., "Semiconductor optical amplifier based photonic logic devices," *Proc. SPIE* **5814**, 1–8 (2005).
7. N. K. Dutta and J. Jaques, "Semiconductor optical amplifier based optical logic devices," *Proc. SPIE* **6014**, 60140X (2005).
8. H. Dong et al., "80 Gb/s all-optical logic AND operation using Mach–Zehnder interferometer with differential scheme," *Opt. Commun.* **265**, 79–83 (2006).
9. A. Sharaiha, J. Topomondzo, and P. Morel, "All-optical logic AND-NOR gates with three inputs based on cross-gain modulation in a semiconductor optical amplifier," *Opt. Commun.* **265**, 322–325 (2006).
10. H. Dong et al., "All-optical logic AND operation at 80 Gb/s using semiconductor optical amplifier based Mach–Zehnder interferometer," *Microwave Opt. Technol. Lett.* **48**, 1672–1675 (2006).
11. Q. Wang et al., "All-optical logic OR gate using SOA delayed interferometer," *Opt. Commun.* **260**, 81–86 (2006).
12. J. Y. Kim et al., "All-optical multiple logic gates with XOR, NOR, OR and NAND function using parallel SOA-MZI structures: theory and experiment," *J. Lightwave Technol.* **24**, 3392–3399 (2006).
13. J. Y. Kim et al., "10 Gbits all-optical composite logic gates with XOR, NOR, OR and NAND functions using SOA-MZI structures," *Electron. Lett.* **42**, 303–307 (2006).

14. J. Dong et al., "40 Gbit/s reconfigurable photonic logic gates based on various nonlinearities in single SOA," *Electron. Lett.* **43**, 884–886 (2007).
15. J. Dong et al., "40 Gb/s all-optical logic NOR and OR gates using a semiconductor optical amplifier: experimental demonstration and theoretical analysis," *Opt. Commun.* **281**, 1710–1715 (2008).
16. J. M. Martínez, F. Ramos, and J. Martí, "10 Gb/s reconfigurable optical logic gate using a single hybrid-integrated SOA-MZI," *Fiber Integr. Opt.* **27**, 15–23 (2008).
17. A. Kotb et al., "Effect of amplified spontaneous emission on semiconductor optical amplifier based all-optical logic," *Opt. Commun.* **284**, 5798–5803 (2011).
18. S. K. Garai, P. Ghosh, and S. Mukhopadhyay, "Analytical approach of developing wavelength encoded AND, NAND and X-OR logic operations and implementation of the theory using semiconductor optical amplifiers," *Optik* **122**, 569–576 (2011).
19. A. Kotb, *All-Optical Logic Gates Using Semiconductor Optical Amplifier*, Lambert Academic Publishing, Saarbrucken (2012).
20. S. Singh and Lovkesh, "Ultrahigh-speed optical signal processing logic based on an SOA-MZI," *IEEE J. Sel. Top. Quantum Electron.* **18**, 970–975 (2012).
21. A. Kotb, "AND-based on two-photon absorption in semiconductor optical amplifier," *Optoelectron. Lett.* **9**, 181–184 (2013).
22. N. K. Dutta and Q Wang. *Semiconductor Optical Amplifiers*, 2nd ed., World Scientific, Singapore (2013).
23. G. Wang, X. Yang, and W. Hu, "All-optical logic gates for 40 Gb/s NRZ signals using complementary data in SOA-MZIs," *Opt. Commun.* **290**, 28–32 (2013).
24. S. Singh, R. Kaur, and R. S. Kaler, "Photonic processing for all-optical logic gates based on semiconductor optical amplifiers," *Opt. Eng.* **53**, 116102 (2014).
25. P. Singh et al., "Design and analysis of all-optical AND, XOR and OR gates based on SOA-MZI configuration," *Opt. Laser Technol.* **66**, 35–44 (2015).
26. Lovkesh and A. Marwaha, "Implementation of optical logic gates at 160 Gbps using nonlinear effect of single SOA," *Opt. Laser Technol.* **70**, 112–118 (2015).
27. A. Kotb and K. E. Zoiros, "Soliton all-optical logic AND gate with semiconductor optical amplifier-assisted Mach–Zehnder interferometer," *Opt. Eng.* **55**, 087109 (2016).
28. A. Kotb, "Numerically simulation of soliton OR gate with semiconductor optical amplifier-assisted delayed interferometer," *Opt. Quantum Electron.* **48**, 462 (2016).
29. I. Rendón-Salgado and R. Gutiérrez-Castrejón, "160 Gb/s all-optical AND gate using bulk SOA turbo-switched Mach–Zehnder interferometer," *Opt. Commun.* **399**, 77–86 (2017).
30. B. Han and Y. Liu, "All-optical reconfigurable non-inverted logic gates with a single semiconductor optical amplifier," *AIP Adv.* **9**, 015007 (2019).
31. B. Han et al., "All-optical non-inverted parity generator and checker based on semiconductor optical amplifiers," *Appl. Sci.* **11**, 1499 (2021).
32. D. R. Zimmerman and L. H. Spiekman, "Amplifiers for the masses: EDFA, EDWA, and SOA amplest for metro and access applications," *J. Lightwave Technol.* **22**, 63–70 (2004).
33. K. E. Zoiros, et al., "Reflective semiconductor optical amplifier pattern effect compensation with birefringent fiber loop," *Opt. Quantum Electron.* **52**, 366 (2020).
34. E. Dimitriadou and K. E. Zoiros, "Proposal for all-optical NOR gate using single quantum-dot semiconductor optical, *Opt. Commun.* **285**, 1710–1716 (2012).
35. Y. Ueno, S. Nakamura, and K. Tajima, "Nonlinear phase shifts induced by semiconductor optical amplifiers with control pulses at repetition frequencies in the 40-160-GHz range for use in ultrahigh-speed all-optical signal processing," *J. Opt. Soc. Am. B* **19**, 2573–2589 (2002).
36. E. Zhou, X. Zhang, and D. Huang, "Analysis on dynamic characteristics of semiconductor optical amplifiers with certain facet reflection based on detailed wideband model," *Opt. Express* **15**, 9096–9106 (2007).
37. B. Schrenk et al., "Direct 10-Gb/s modulation of a single-section RSOA in PONs with high optical budget," *IEEE Photonics Technol. Lett.* **22**, 392–394 (2010).
38. Z. V. Rizou and K. E. Zoiros, "Theoretical analysis of directly modulated reflective semiconductor optical amplifier performance enhancement by microring resonator-based notch filtering," *Appl. Sci.* **8**, 223 (2018).

39. Z. V. Rizou et al., "Reflective semiconductor optical amplifier direct modulation capability enhancement using birefringent fiber loop," *Appl. Sci.* **10**, 5328 (2020).
40. R. Paiella et al., "Wavelength conversion by four-wave mixing in a folded-path, self-pumped semiconductor optical amplifier," in *Proc. Opt. Fiber Commun.*, pp. 109–110 (1998).
41. Y. Maeda and L. Occhi, "All-optical triode based on a tandem wavelength converter using reflective semiconductor optical amplifiers," *IEEE Photonics Technol. Lett.* **15**, 257–259 (2003).
42. L. Q. Guo and M. J. Connelly, "A novel approach to all-optical wavelength conversion by utilizing a reflective semiconductor optical amplifier in a co-propagation scheme," *Opt. Commun.* **281**, 4470–4473 (2008).
43. C. S. Reis, "All-optical routing functionalities," PhD Thesis, University of Aveiro, Portugal (2014).
44. A. Mukherjee, "A novel frequency encoded all-optical logic gates exploiting polarization insensitive four-wave mixing in semiconductor optical amplifier, filtering property of ADD/DROP multiplexer and non-linearity of reflective semiconductor amplifier," *Optik* **122**, 891–895 (2011).
45. P. P. Sarkar, B. Ghosh, and S. N. Patra, "Simulative study of all optical frequency encoded debit based universal NAND and NOR logic gates using a reflective semiconductor optical amplifier and an add/drop multiplexer," *J. Opt. Technol.* **83**, 257–262 (2016).
46. A. Kotb, K. E. Zoiros, and C. Guo, Performance investigation of 120 Gb/s all-optical logic XOR gate using dual-reflective semiconductor optical amplifier-based scheme, *J. Comput. Electron.* **17**, 1640–1649 (2018).
47. A. Kotb and C. Guo, "120 Gb/s all-optical NAND logic gate using reflective semiconductor optical amplifiers," *J. Mod. Opt.* **67**, 1138–1144 (2020).
48. A. Kotb and C. Guo, "Reflective semiconductor optical amplifiers-based all-optical NOR and XNOR logic gates at 120 Gb/s," *J. Mod. Opt.* **67**, 1424–1435 (2020).
49. M. J. Connelly, "Reflective semiconductor optical amplifier pulse propagation model," *IEEE Photonics Technol. Lett.* **24**, 95–97 (2012).
50. I. Sengupta and A. D. Barman, "Analysis of optical re-modulation by multistage modeling of RSOA," *Optik* **125**, 3393–3400 (2014).
51. S. P. Ó Dúill and L. P. Barry, "Improved reduced models for single-pass and reflective semiconductor optical amplifiers," *Opt. Commun.* **334**, 170–173 (2015).
52. C. Antonelli and A. Mecozzi, "Reduced model for the nonlinear response of reflective semiconductor optical amplifiers," *IEEE Photonics Technol. Lett.* **25**, 2243–2246 (2013).
53. C. Antonelli et al., "Analytic study of the modulation response of reflective semiconductor optical amplifiers," *J. Lightwave Technol.* **33**, 4367–4376 (2015).
54. D. Cassioli, S. Scotti, and A. Mecozzi, "A time-domain computer simulator of the nonlinear response of semiconductor optical amplifiers," *IEEE J. Quantum Electron.* **36**, 1072–1080 (2000).
55. J. Leuthold et al., "All-optical space switches with gain and principally ideal extinction ratios," *IEEE J. Quantum Electron.* **34**, 622–633 (1998).
56. N. C. Harris et al., "Efficient, compact and low loss thermo-optic phase shifter in silicon," *Opt. Express* **22**, 10487–10493 (2014).
57. J. D. LeGrange et al., "Cascaded all-optical operations in a hybrid integrated 80-Gb/s logic circuit," *Opt. Express* **22**, 13600–13615 (2014).
58. K. E. Zoiros and C. Demertzis, "On the data rate extension of semiconductor optical amplifier-based ultrafast nonlinear interferometer in dual rail switching mode using a cascaded optical delay interferometer," *Opt. Laser Technol.* **43**, 1190–1197 (2011).
59. R. Bonk et al., "The input power dynamic range of a semiconductor optical amplifier and its relevance for access network applications," *IEEE Photonics* **3**, 1039–1053 (2011).
60. A. M. Melo and K. Petermann, "On the amplified spontaneous emission noise modeling of semiconductor optical amplifiers," *Opt. Commun.* **281**, 4598–4605 (2008).
61. K. Morishita, "Wavelength-selective optical-fiber directional couplers using dispersive materials," *Opt. Lett.* **13**, 158–160 (1988).

62. A. Kotb, K. E. Zoiros, and C. Guo, All-optical XOR, NOR, and NAND logic functions with parallel semiconductor optical amplifier-based Mach–Zehnder interferometer modules," *Opt. Laser Technol.* **108**, 426–433 (2018).
63. T. Akiyama et al., "Nonlinear processes responsible for non-degenerate four-wave mixing in quantum dot optical amplifiers," *Appl. Phys. Lett.* **77**, 1753–1755 (2000).
64. J. Xu, X. Zhang, and J. Mørk, "Investigation of patterning effects in ultrafast SOA-based optical switches," *IEEE J. Quantum Electron.* **46**, 87–94 (2010).
65. J. S. Vardakas and K. E. Zoiros, "Performance investigation of all-optical clock recovery circuit based on Fabry–Pérot filter and SOA-assisted Sagnac switch," *Opt. Eng.* **46**, 085005 (2007).
66. G. Papadopoulos and K. E. Zoiros, "On the design of semiconductor optical amplifier-assisted Sagnac interferometer with full data dual output switching capability," *Opt. Laser Technol.* **43**, 697–710 (2011).
67. S. Ó Dúill et al., "Efficient modulation cancellation using reflective SOAs," *Opt. Express* **20**, 587–594 (2012).
68. L. Schares et al., "Phase dynamics of semiconductor optical amplifiers at 10 to 40 GHz," *IEEE J. Quantum Electron.* **39**, 1394–1408 (2003).
69. T. Siarkos, K. E. Zoiros, and D. Nastou, "On the feasibility of full pattern-operated all-optical XOR gate with single semiconductor optical amplifier-based ultrafast nonlinear interferometer," *Opt. Commun.* **282**, 2729–2734 (2009).
70. H. C. H. Mulvad et al., "Demonstration of 5.1 Tb/s data capacity on a single-wavelength channel," *Opt. Express* **18**, 1438–1443 (2010).
71. L. H. Spiekman, "Active devices in passive optical networks," *J. Lightwave Technol.* **31**, 488–497 (2013).

Biographies of the authors are not available.